

Shear viscosity of pionic and nucleonic components from their different possible mesonic and baryonic thermal fluctuations

Sabyasachi Ghosh

Received: date / Accepted: date

Abstract Owing to the Kubo relation, the shear viscosities of pionic and nucleonic components have been evaluated from their corresponding retarded correlators of viscous stress tensor in the static limit, which become non-divergent only for the non-zero thermal widths of the constituent particles. In the real-time thermal field theory, the pion and nucleon thermal widths have respectively been obtained from the pion self-energy for different meson, baryon loops and the nucleon self-energy for different pion-baryon loops. We have found a non-monotonic momentum distributions of pion and nucleon thermal widths, which have been integrated out by their respective Bose-enhanced and Pauli-blocked phase space factors during evaluation of their shear viscosities. The viscosity to entropy density ratio for this mixed gas of pion-nucleon system decreases and approaches toward its lower bound as the temperature and baryon chemical potential increase within the relevant domain of hadronic matter.

1 Introduction

A strongly interacting matter is expected to be produced, instead of a weakly interacting gas, at RHIC and LHC energies as the shear viscosity of the matter thus produced is exposed to be very small. This was concluded by the hydrodynamical simulations [1,2,3,4,5,6] as well as some transport calculations [7,8,9,10] to explain the elliptic flow parameter observed at RHIC and LHC. According to the investigations conducted in Refs. [11,12,13,14,15,16,17], the shear viscosity to entropy density ratio, η/s may reach a minimum in the vicinity of a phase transition, which is also indicated by some lattice QCD calculations[18,19,20]. The minimum value of η/s may be very close to its quantum lower bound, commonly known as

This work is financed by Fundação de Amparo à Pesquisa do Estado de São Paulo - FAPESP, Grant Nos. 2012/16766-0.

Sabyasachi Ghosh
Instituto de Física Teórica, Universidade Estadual Paulista, Rua Dr. Bento Teobaldo Ferraz,
271 - Bloco II, 01140-070 São Paulo, SP, Brazil
E-mail: sabyaphy@gmail.com

the KSS bound [21]. Owing to these interesting issues, a growing interest in the microscopic calculation of shear viscosity for the QGP phase [22, 23, 24, 25, 26, 27] and hadronic phase [28, 29, 30, 31, 32, 33, 34, 35, 36, 37, 38, 39, 40, 41, 42, 43, 44, 45, 46] has been noticed in recent times, though the transport coefficient calculations of nuclear matter started somewhat earlier [47, 48, 49, 50, 51, 52]. Importance of knowing the explicit temperature dependence of shear viscosity for hadronic phase has been pointed out in a recent work by Niemi et al. [4]. They have shown that the extracted transverse momentum p_T dependence of elliptic flow parameter, $v_2(p_T)$, of RHIC data is highly sensitive to the temperature dependent η/s in hadronic matter and almost independent of the viscosity in the QGP phase.

Being inspired by this, we have studied the shear viscosity of pionic medium [53] and then extended our study to the pion-nucleon system [54]. To calculate shear viscosity of the pionic component via Kubo relation [55, 56], the thermal correlator of viscous stress tensor for pionic constituents has to be derived, where a finite thermal width of pion should be included for getting a non-divergent value of correlator in the static limit [32, 40, 57]. In Ref. [53], the pion thermal width is estimated from the pion self-energy for different mesonic loops, which are obtained in the formalism of real-time thermal field theory (RTF). Similarly, the thermal correlator of viscous stress tensor for nucleonic constituents is obtained in Ref. [54] to calculate the shear viscosity of nucleonic component, where different pion-baryon loops are taken into account to determine the nucleon thermal width. Now, in the two component nucleon-pion system, pion propagation may also have some baryonic fluctuations besides the mesonic fluctuations. This contribution, which was absent in our previous studies [53, 54], is considered in the present work to revisit our shear viscosity calculation for two component nucleon-pion system.

In the next section, the formalism of shear viscosity for pionic and nucleonic components are briefly described, where their corresponding thermal widths are discussed in three different subsections. In the subsection 2.1, we have elaborately deduced the pion thermal width in baryonic medium by calculating the pion self-energy for different baryonic loops in the formalism of RTF. In the next two subsections, the relevant expressions of pion thermal width due to different mesonic loops and nucleon thermal width from different pion-baryon loops are briefly addressed as the detailed deduction of these expressions are already provided in the previous studies [53, 54]. The numerical outcomes are discussed in Sec. 3 and in Sec. 4, we have summarized and concluded this article.

2 Formalism

Owing to the famous Kubo formula [55, 56], the spectral function of two point viscous-stress tensor, $\pi^{\mu\nu}$ can determine the shear viscosity in momentum space by the standard relation [32]

$$\eta = \frac{1}{20} \lim_{q_0, \mathbf{q} \rightarrow 0} \frac{1}{q_0} \int d^4x e^{iq \cdot x} \langle [\pi_{ij}(x), \pi^{ij}(0)] \rangle_\beta, \quad (1)$$

where $\langle \hat{O} \rangle_\beta$ for any operator \hat{O} denotes the equilibrium ensemble average; $\langle \hat{O} \rangle_\beta = \frac{\text{Tr} e^{-\beta H} \hat{O}}{\text{Tr} e^{-\beta H}}$.

The simplest one-loop expressions of Eq. (1) for pion and nucleon degrees of freedom are respectively given below [57]

$$\eta_\pi = \frac{\beta I_\pi}{30\pi^2} \int_0^\infty \frac{d\mathbf{k}\mathbf{k}^6}{\omega_k^{\pi^2} \Gamma_\pi} n_k(\omega_k^\pi) \{1 + n_k(\omega_k^\pi)\} \quad (2)$$

and

$$\eta_N = \frac{\beta I_N}{15\pi^2} \int_0^\infty \frac{d\mathbf{k}\mathbf{k}^6}{\omega_k^{N^2} \Gamma_N} [n_k^+(\omega_k^N) \{1 - n_k^+(\omega_k^N)\} + n_k^-(\omega_k^N) \{1 - n_k^-(\omega_k^N)\}] . \quad (3)$$

Their schematic diagrams are shown in Fig. 1(a) and 2(a) respectively. Hence, adding the pionic and nucleonic components, we get the total shear viscosity

$$\eta_\Gamma = \eta_\pi + \eta_N . \quad (4)$$

In the above equations, $n_k(\omega_k^\pi) = 1/\{e^{\beta\omega_k^\pi} - 1\}$ is Bose-Einstein (BE) distribution of pion with energy $\omega_k^\pi = (\mathbf{k}^2 + m_\pi^2)^{1/2}$ whereas $n_k^\pm = 1/\{e^{\beta(\omega_k^\pm \mp \mu_N)} + 1\}$ are Fermi-Dirac (FD) distributions of nucleon and anti-nucleon with energy $\omega_k^N = (\mathbf{k}^2 + m_N^2)^{1/2}$. The corresponding thermal widths, Γ_π and Γ_N for pion and nucleon can be defined as

$$\begin{aligned} \Gamma_\pi &= \sum_B \Gamma_{\pi(NB)} + \sum_M \Gamma_{\pi(\pi M)} \\ &= - \sum_B \text{Im} \Pi_{\pi(NB)}^R(k_0 = \omega_k^\pi, \mathbf{k})/m_\pi - \sum_M \text{Im} \Pi_{\pi(\pi M)}^R(k_0 = \omega_k^\pi, \mathbf{k})/m_\pi \end{aligned} \quad (5)$$

and

$$\Gamma_N = \sum_B \Gamma_{N(\pi B)} = - \sum_B \text{Im} \Sigma_{N(\pi B)}^R(k_0 = \omega_k^N, \mathbf{k}) \quad (6)$$

respectively, where $\Pi_{\pi(NB)}^R(k)$ is pion self-energy for different nucleon-baryon (NB) loops (shown in Fig. 1(c) and (d)), $\Pi_{\pi(\pi M)}^R(k)$ is pion self-energy for different pion-meson (πM) loops (shown in Fig. 1(b)) and $\Sigma_{N(\pi B)}^R(k)$ is nucleon self-energy for different pion-baryon (πB) loops (shown in Fig. 2(b)). The superscript R stands for retarded component of self-energy and subscripts represent the external (outside the bracket) and internal (inside the bracket) particles for the corresponding self-energy graphs as shown in Fig. 1(b), (c), (d) and Fig. 2(b). Adoption of finite thermal widths Γ_π and Γ_N in Eq. (2) and (3) respectively is a very well established technique [32, 40], which is generally used in Kubo approach to get a non-divergent value of the shear viscosity coefficient. In this respect this treatment is equivalent to quasi-particle approximation or relaxation time approximation. Again, this one-loop expression of η_π or η_N from Kubo approach [32, 40, 58] exactly coincides with the expression coming from the relaxation-time approximation of the kinetic theory approach [47, 48, 41, 58]. Hence, the thermal width of medium constituent plays a vital role in determining the numerical strength of shear viscosity of the medium.

Next we discuss the calculations of thermal widths from different one-loop self-energy graphs as shown in Fig. (1) and (2).

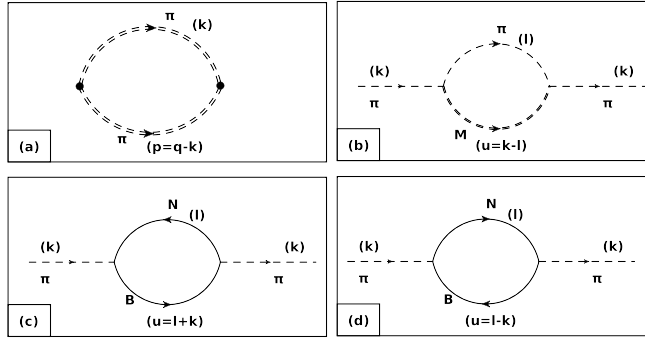


Fig. 1 The diagram (a) is a schematic one-loop representation of viscous-stress tensor for the medium with pionic constituents. The double dashed lines for the pion propagators indicate that they have some finite thermal width, which can be derived from the pion self-energy diagrams (b), (c) and (d). The diagram (b) represents pion self-energy for mesonic (πM) loops. Direct and cross diagrams of pion self-energy for NB loops are represented by (c) and (d) respectively.

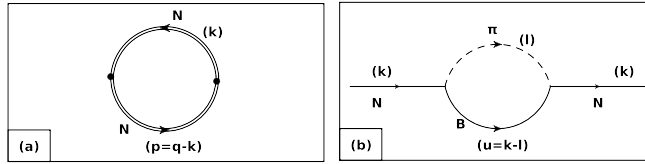


Fig. 2 The diagram (a) is a schematic one-loop representation of viscous-stress tensor for the medium with nucleonic constituents and the diagram (b) represents nucleon self-energy for πB loops.

2.1 Pion thermal width for different baryonic loops

Let us first concentrate on the pion self-energy calculations for different possible baryon loops *i.e.* $\Pi_{\pi(NB)}^R$. During propagation in the medium, pion propagator can undergo different intermediate NB loops, where $B = \Delta(1232)$, $N^*(1440)$, $N^*(1520)$, $N^*(1535)$, $\Delta^*(1600)$, $\Delta^*(1620)$, $N^*(1650)$, $\Delta^*(1700)$, $N^*(1700)$, $N^*(1710)$, $N^*(1720)$ are accounted in this work. The masses of all the 4-star baryon resonances (in MeV) are presented inside the brackets. The direct and cross diagrams of pion self-energy for NB loops have been represented in the diagrams 1(c) and (d).

In real-time formalism of thermal field theory (RTF), self-energy becomes 2×2 matrix with 11, 12, 21 and 22 components. From any of the components, one can find the retarded part of self-energy, which is directly related with physical quantity - thermal width (inverse of thermal relaxation time). Let us start with the 11-component of in-medium pion self-energy for NB loop :

$$\Pi_{\pi(NB)}^{11}(k) = i \sum_{a=-1,+1} \int \frac{d^4 l}{(2\pi)^4} L(k, l) E_N^{11}(l) E_B^{11}(l - ak) \quad (7)$$

where $E_N^{11}(l)$ and $E_B^{11}(l - ak)$ are scalar parts of the nucleon and baryon propagators respectively at finite temperature. In RTF this expression is as follows

$$E_N^{11}(l) = \frac{-1}{l^2 - m_N^2 + i\eta} - 2\pi i \{n_l^+ \theta(l_0) + n_l^- \theta(-l_0)\} \delta(l^2 - m_N^2), \quad (8)$$

where $n_l^\pm(\omega_l^N) = 1/\{e^{\beta(\omega_l^N \mp \mu_N)} + 1\}$ are the FD distributions of nucleon and anti-nucleon for energy $\omega_l^N = (l^2 + m_N^2)^{1/2}$ and μ_N is the chemical potential of nucleon which is supposed to be equal with the chemical potentials of all the baryons considered here. The two values of a in Eq. (7) correspond to the direct and crossed diagrams, shown in Fig. 1 (c) and (d) respectively, which can be obtained from one another by changing the sign of external momentum k .

Let us first discuss diagram (d) for which $a = +1$. Integrating Eq. (7) over l^0 and using the relation,

$$\text{Im}\Pi_{\pi(NB)}^R(k) = \tanh(\beta k_0/2) \text{Im}\Pi_{\pi(NB)}^{11}(k), \quad (9)$$

the retarded component of the in-medium self energy (imaginary part) can be expressed as

$$\begin{aligned} \text{Im}\Pi_{\pi(NB)}^R(k) = \pi\epsilon(k_0) \int \frac{d^3l}{(2\pi)^3} \frac{1}{4\omega_l^N \omega_u^B} \\ L_1[\{1 - n_l^+(\omega_l^N) - n_u^-(\omega_u^B)\} \delta(k_0 - \omega_l^N - \omega_u^B) \\ + \{n_l^+(\omega_l^N) - n_u^+(\omega_u^B)\} \delta(k_0 - \omega_l^N + \omega_u^B)] \\ + L_2[\{-n_l^-(\omega_l^N) + n_u^-(\omega_u^B)\} \delta(k_0 + \omega_l^N - \omega_u^B) \\ + \{-1 + n_l^-(\omega_l^N) + n_u^+(\omega_u^B)\} \delta(k_0 + \omega_l^N + \omega_u^B)], \quad (10) \end{aligned}$$

where $n_u^\pm(\omega_u^B) = 1/\{e^{\beta(\omega_u^B \mp \mu_N)} + 1\}$ are also FD distribution functions for baryon and anti-baryon with $\omega_u^B = \{(1 - \mathbf{k})^2 + m_B^2\}^{1/2}$ and $L_{1,2}$ denote the values of $L(l_0, \mathbf{l}, k)$ for $l_0 = \omega_l^N$ and $-\omega_l^N$ respectively. The different δ functions in Eq. (10) create the regions of different branch cuts in k_0 -axis viz. $-\infty$ to $-\{\mathbf{k}^2 + (m_N + m_B)^2\}^{1/2}$ for unitary cut in negative k_0 -axis, $-\{\mathbf{k}^2 + (m_B - m_N)^2\}^{1/2}$ to $\{\mathbf{k}^2 + (m_B - m_N)^2\}^{1/2}$ for Landau cut and $\{\mathbf{k}^2 + (m_N + m_B)^2\}^{1/2}$ to ∞ for unitary cut in positive k_0 -axis. In these different kinematic regions, the imaginary part of the pion self-energy becomes non-zero. Among the four terms in the right hand side of Eq. (10), the third term contributes in pion thermal width for baryonic loops, $\Gamma_{\pi(NB)}$ because the pion pole ($k_0 = \omega_k^\pi, \mathbf{k}$) is situated within the Landau cut (0 to $\{\mathbf{k}^2 + (m_B - m_N)^2\}^{1/2}$) in the positive k_0 -axis. From the Eq. (5), using the relation,

$$\Gamma_{\pi(NB)} = -\text{Im}\Pi_{\pi(NB)}^R(k_0 = \omega_k^\pi, \mathbf{k})/m_\pi \quad (11)$$

and adding the relevant Landau cut contributions of both diagrams (c) and (d), the total thermal width of pion for any NB loop is given by

$$\begin{aligned} \Gamma_{\pi(NB)}(\mathbf{k}, T, \mu_N) = \frac{1}{16\pi|\mathbf{k}|m_\pi} \int_{\omega_{l_+}^N}^{\omega_{l_-}^N} d\omega_l^N \times L(l_0 = -\omega_l^N, \mathbf{l}, k_0 = \omega_k^\pi, \mathbf{k}) [\{-n_l^+(\omega_l^N) \\ + n_u^+(\omega_u^B = \omega_k^\pi + \omega_l^N)\} + \{-n_l^-(\omega_l^N) + n_u^-(\omega_u^B = \omega_k^\pi + \omega_l^N)\}], \quad (12) \end{aligned}$$

where

$$\omega_{l\pm}^N = \frac{S_{\pi(NB)}^2}{2m_\pi^2} (-\omega_k^\pi \pm |\mathbf{k}| W_{\pi(NB)}), \quad (13)$$

with

$$S_{\pi(NB)}^2 = m_\pi^2 - m_B^2 + m_N^2 \quad (14)$$

and

$$W_{\pi(NB)} = (1 - 4m_\pi^2 m_N^2 / S_{\pi(NB)}^4)^{1/2}. \quad (15)$$

Lagrangian densities of spin $J_B = 1/2$ and $3/2$ baryons can be written as

$$\mathcal{L}_{\text{Baryon}} = \sum_B \left[\mathcal{L}_{B(J_B=1/2,3/2)}^{\text{free}} + \mathcal{L}_{B(J_B=1/2,3/2)}^{\text{int}} \right], \quad (16)$$

where free parts of Lagrangian densities for baryonic fields with spin $J_B = 1/2$ and $J_B = 3/2$ are

$$\begin{aligned} \mathcal{L}_{B(J_B=1/2)}^{\text{free}} &= \sum_{B(J_B=1/2)} \bar{\psi}_B (i\gamma^\mu \partial_\mu - m_B) \psi_B, \\ \mathcal{L}_{B(J_B=3/2)}^{\text{free}} &= \sum_{B(J_B=3/2)} -\frac{1}{2} \bar{\psi}_B^\mu (\epsilon_{\mu\nu\alpha\beta} \gamma^\alpha \partial^\beta - im_B \sigma^{\alpha\beta}) \psi_B^\nu \\ &\quad \text{with } \sigma^{\alpha\beta} = \frac{i}{2} [\gamma^\alpha, \gamma^\beta] \end{aligned} \quad (17)$$

and their interaction parts are [59],

$$\begin{aligned} \mathcal{L}^{\text{int}} &= \frac{f}{m_\pi} \bar{\psi}_B \gamma^\mu \left\{ \begin{array}{c} i\gamma^5 \\ \mathbb{1} \end{array} \right\} \psi_N \partial_\mu \pi + \text{h.c. for } J_B^P = \frac{1}{2}^\pm, \\ \mathcal{L}^{\text{int}} &= \frac{f}{m_\pi} \bar{\psi}_B^\mu \left\{ \begin{array}{c} \mathbb{1} \\ i\gamma^5 \end{array} \right\} \psi_N \partial_\mu \pi + \text{h.c. for } J_B^P = \frac{3}{2}^\pm, \end{aligned} \quad (18)$$

Here P stands for parity quantum numbers of the baryons. The coupling constants πNB interactions are fixed from the experimental decay widths of $B \rightarrow N\pi$ channels [60]. They are $f/m_\pi = 15.7, 2.5, 11.6, 1.14, 3.4, 1.22, 1.14, 9.5, 2.8, 0.35$ and 1.18 for $\Delta(1232), N^*(1440), N^*(1520), N^*(1535), \Delta^*(1600), \Delta^*(1620), N^*(1650), \Delta^*(1700), N^*(1700), N^*(1710), N^*(1720)$. Using (18), we have found the vertex factors [60]:

$$\begin{aligned} L(k, l) &= -4 \left(\frac{f}{m_\pi} \right)^2 [2(k \cdot l)^2 - a(k \cdot l)k^2 - k^2(l^2 + m_N m_B)], \quad \text{for } J_B^P = \frac{1}{2}^\pm, \\ &= -\frac{8}{3m_B^2} \left(\frac{f}{m_\pi} \right)^2 [m_N m_B + l^2 - a(k \cdot l)][(l \cdot k - ak^2)^2 - k^2 m_B^2], \\ &\quad \text{for } J_B^P = \frac{3}{2}^\pm. \end{aligned} \quad (19)$$

2.2 Pion thermal width for different mesonic loops

To calculate the mesonic loop contribution of pionic thermal width $\Gamma_{\pi(\pi M)}$, we have evaluated pion self-energy for πM loops, where M stands for σ and ρ mesons. This contribution estimated in our previous work [53] elaborately. Following that [53], the expression of pion thermal width from the mesonic loops is given below

$$\Gamma_{\pi(\pi M)}(\mathbf{k}, T) = \frac{1}{16\pi|\mathbf{k}|m_\pi} \int_{\omega_{i+}^\pi}^{\omega_{i-}^\pi} d\omega_l^\pi L(l_0 = -\omega_l^\pi, \mathbf{l}, k_0 = \omega_k^\pi, \mathbf{k}) \{n_l(\omega_l^\pi) - n_u(\omega_u^M = \omega_k^\pi + \omega_l^\pi)\}, \quad (20)$$

where n_l, n_u are BE distribution functions of π, M mesons respectively and the limits of integration are

$$\omega_{l\pm}^\pi = \frac{S_{\pi(\pi M)}^2}{2m_\pi^2} (-\omega_k^\pi \pm |\mathbf{k}| W_{\pi(\pi M)}), \quad (21)$$

with

$$S_{\pi(\pi M)}^2 = 2m_\pi^2 - m_M^2 \quad (22)$$

and

$$W_{\pi(\pi M)} = (1 - 4m_\pi^4/S_{\pi(\pi M)}^4)^{1/2}. \quad (23)$$

Lagrangian density of pion, sigma and rho mesons can be written as

$$\mathcal{L} = \mathcal{L}_\pi^{\text{free}} + \mathcal{L}_\sigma^{\text{free}} + \mathcal{L}_\rho^{\text{free}} + \mathcal{L}_{\pi\pi\rho}^{\text{int}} + \mathcal{L}_{\pi\pi\sigma}^{\text{int}}, \quad (24)$$

where free parts of Lagrangian densities for pseudo-scalar π , scalar σ and vector ρ^μ fields are are

$$\begin{aligned} \mathcal{L}_\pi^{\text{free}} &= \frac{1}{2} \{(\partial_\mu \pi) \cdot (\partial^\mu \pi) - m_\pi^2 \pi^2\} \\ \mathcal{L}_\sigma^{\text{free}} &= \frac{1}{2} \{(\partial\sigma)^2 - m_\sigma^2 \sigma^2\} \\ \mathcal{L}_\rho^{\text{free}} &= \frac{1}{2} \{(\rho_{\mu\nu} \rho^{\mu\nu}) - m_\rho^2 (\rho_\mu \rho^\mu)\}, \quad \rho^{\mu\nu} = (\partial^\mu \rho^\nu - \partial^\nu \rho^\mu) \end{aligned} \quad (25)$$

and their interaction parts are [61, 53, 41]

$$\begin{aligned} \mathcal{L}_{\pi\pi\rho}^{\text{int}} &= g_\rho \rho_\mu \cdot \pi \times \partial^\mu \pi \\ \mathcal{L}_{\pi\pi\sigma}^{\text{int}} &= \frac{g_\sigma}{2} m_\sigma \pi \cdot \pi \sigma. \end{aligned} \quad (26)$$

The coupling constant $g_\rho = 6$ and $g_\sigma = 5.82$ are fixed from experimental decay width [53] and physical masses of pion, sigma and rho mesons are taken as $m_\pi = 0.140$ GeV, $m_\sigma = 0.390$ GeV and $m_\rho = 0.770$ GeV. Using (26) we have obtained the vertex factors:

$$\begin{aligned} L(k, l) &= -\frac{g_\sigma^2 m_\sigma^2}{4}, \quad \text{for } M = \sigma, \\ &= -\frac{g_\rho^2}{m_\rho^2} [k^2 (k^2 - m_\rho^2) + l^2 (l^2 - m_\rho^2) - 2\{(k \cdot l) m_\rho^2 + k^2 l^2\}], \quad \text{for } M = \rho. \end{aligned} \quad (27)$$

2.3 Nucleon thermal width

In order to calculate the nucleonic thermal width $\Gamma_{N(\pi B)}$, we have evaluated nucleon self-energy for different possible πB loops, where B stands for all the baryons as taken in pion self-energy for baryonic loops. This contribution is rigorously addressed in our previous work [54]. Hence taking the relevant expression of nucleon thermal width for any πB loop from the Ref. [54], we have

$$\Gamma_{N(\pi B)}(\mathbf{k}, T, \mu_N) = \frac{1}{16\pi|\mathbf{k}|m_\pi} \int_{\omega_{i^+}^\pi}^{\omega_{i^-}^\pi} d\omega_i^\pi L \left(l_0 = -\omega_i^\pi, \mathbf{l}, k_0 = \omega_k^N, \mathbf{k} \right) \{n_l(\omega_i^\pi) + n_u(\omega_u^B = \omega_k^N + \omega_i^\pi)\}, \quad (28)$$

where n_l and n_u are BE and FD distribution functions for π and B respectively. The relevant limits of integration in Eq. (28) are:

$$\omega_{i^\pm}^N = \frac{S_{N(\pi B)}^2}{2m_N^2} \left(-\omega_k^N \pm |\mathbf{k}| W_{N(\pi B)} \right), \quad (29)$$

with

$$S_{N(\pi B)}^2 = m_N^2 - m_B^2 + m_\pi^2 \quad (30)$$

and

$$W_{N(\pi B)} = \left(1 - 4m_N^2 m_\pi^2 / S_{N(\pi B)}^4 \right)^{1/2}. \quad (31)$$

The vertex factors [54]:

$$L(k, l) = - \left(\frac{f}{m_\pi} \right)^2 \left\{ \left(\frac{R^2}{2} - m_\pi^2 \right) l_0 - P m_\pi^2 m_B \right\} \text{ for } J_B^P = \frac{1^\pm}{2},$$

$$L(k, l) = - \left(\frac{f}{m_\pi} \right)^2 \frac{2}{3m_B^2} \left\{ \left(\frac{R^2}{2} - m_\pi^2 \right)^2 - m_\pi^2 m_B^2 \right\} (k_0 - l_0 + P m_B) \text{ for } J_B^P = \frac{3^\pm}{2} \quad (32)$$

can be deduced by using the πNB interaction Lagrangian densities from Eq. (18).

3 Results and Discussion

The detailed Landau cut contributions of pion self-energy for mesonic loops and nucleon self-energy for different πB loops are investigated in the earlier Refs. [53] and [54], where their corresponding contributions in the shear viscosity are also addressed. Now in the two component pion-nucleon system, another contribution to pion thermal width can arise from the pion self-energy with baryonic loops, which was not considered in our previous studies of the shear viscosity [53, 54]. The main purpose of the present work is to include these baryonic loop contributions in the pion thermal width and to revisit the shear viscosity results.

Let us first zoom in our attention on the $\Gamma_{\pi(NB)}$. Fig. (3) represents the Landau cut contributions of different NB loops on the invariant mass axis M_k , which can be numerically generated by replacing $\omega_k^\pi = (\mathbf{k}^2 + M_k^2)^{1/2}$ in Eq. (12). For a fixed set of parameters \mathbf{k} , T and μ_N , the $\Gamma_{\pi(NB)}(M_k)$ for baryons $B = \Delta(1232)$,

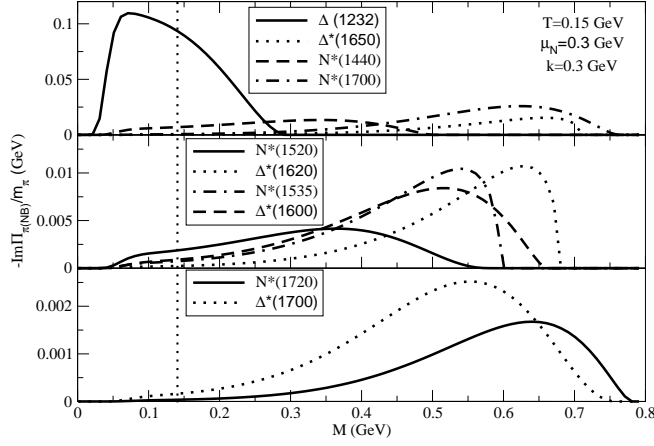


Fig. 3 $\Gamma_{\pi(NB)}(M_k)$ for different NB loops in their Landau regions, which contain the pion pole $M_k = m_\pi$, denoted by straight dotted line.

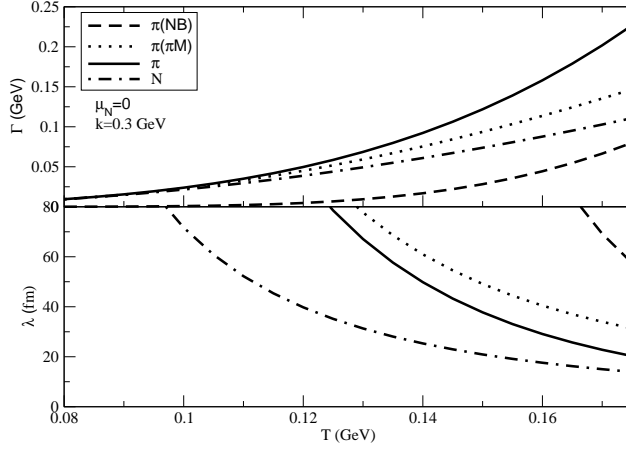


Fig. 4 The on-shell thermal widths (upper panel) and mean free paths (lower panel) of pion for πM loops, NB loops and their total are represented by dotted, dashed and solid lines respectively while dash-dotted line denotes the same results for nucleon component with all possible πB loops.

$\Delta^*(1650)$, $N^*(1440)$, $N^*(1700)$ in the upper panel, $B = N^*(1520)$, $\Delta^*(1620)$, $N^*(1535)$, $\Delta^*(1600)$ in the middle panel and $B = N^*(1720)$, $\Delta^*(1700)$ in the lower panel are individually presented in the Fig. (3). The Landau cut regions, where $\Gamma_{\pi(NB)}(M_k)$ for different NB loops have attained their non-zero values, are clearly observed in the invariant mass axis. As an example, for $N\Delta$ loop the Landau region is from $M = 0$ to $(m_\Delta - m_N) = 0.292$ GeV. The straight dotted line denotes position of pion pole (i.e. $M_k = m_\pi$), which indicates the on-shell contribution of $\Gamma_{\pi(NB)}$ for different baryonic loops. Here we identify $N\Delta$ loop as a leading candidate to contribute in the pion thermal width among all the baryonic loops.

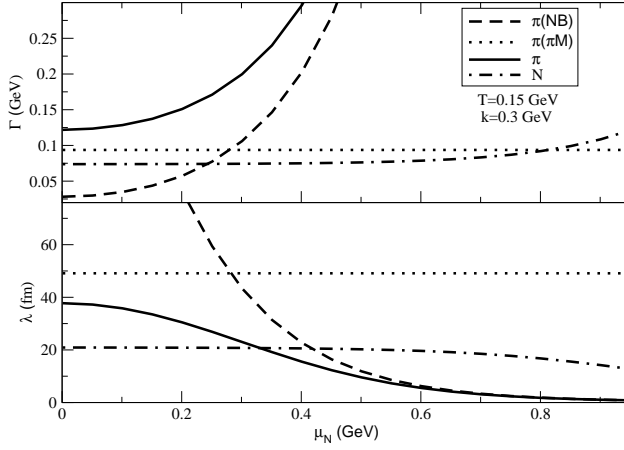


Fig. 5 Same as Fig. (4) along the μ_N axis.

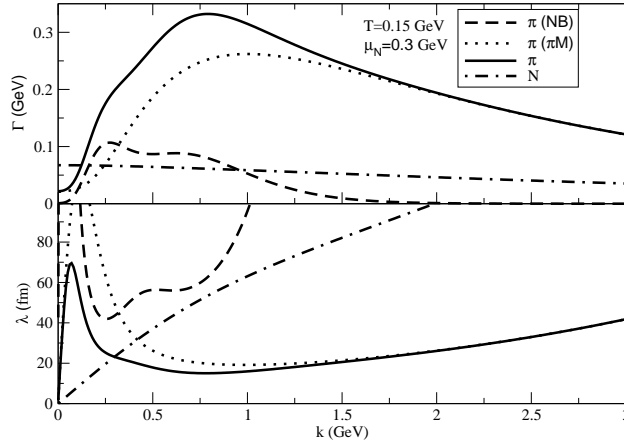


Fig. 6 Same as Fig. (4) along the \mathbf{k} axis

Adding the on-shell contribution of all NB loops, we get the total thermal width of pion for baryonic loops, which is plotted against temperature by dashed line in the upper panel of Fig. (4). Using Eqs.(20) and (28), we have also generated the numerical values of total $\Gamma_{\pi(\pi M)}(T)$ (dotted line) and $\Gamma_{N(\pi B)}(T)$ (dashed line) by adding their corresponding loop contributions for a same set of input parameters ($\mathbf{k} = 0.3$ GeV, $\mu_N = 0$). Following Eq. (5), the solid line represents the T dependence of total thermal width of pion, $\Gamma_{\pi}(T)$ after adding the mesonic and baryonic loop contributions. All of the Γ 's are monotonically increasing function but with different rate of increment. The corresponding results of mean free path, defined by $\lambda = \mathbf{k}/(\omega_k \Gamma)$, are presented in the lower panel of the Fig. (4). Being inversely proportional to the thermal width, the mean free paths for all of the components monotonically decrease with T and exhibit divergent nature at low T . Along the μ_N axis, λ 's (Γ 's) for all of the components also decrease (increase) with

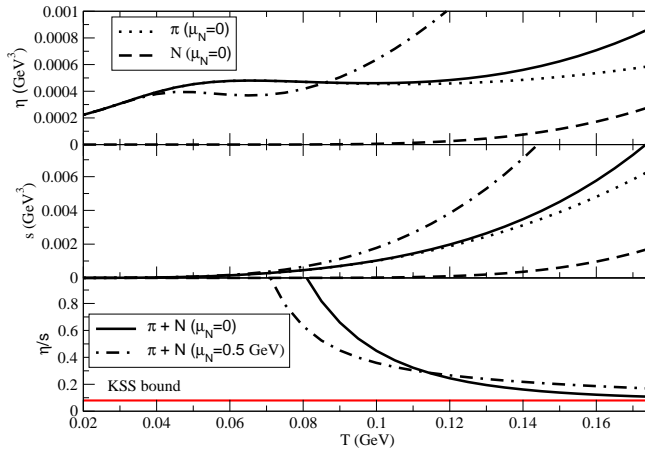


Fig. 7 Temperature dependence of shear viscosities (upper panel) and entropy densities (middle panel) for pionic (dotted line), nucleonic (dashed line) components and their total at two different nucleon chemical potentials: $\mu_N = 0$ (solid line) and $\mu_N = 0.5$ GeV (dash-dotted line). In the lower panel, the ratios of total viscosity to entropy density are represented as a function of T at same set of μ_N 's, taken in the upper and middle panels.

different rates as shown in the lower (upper) panel of Fig. (5). Here we see that independent nature of pion thermal width ($\Gamma_{\pi(\pi M)}$) or mean free path ($\lambda_{\pi(\pi M)}$) for mesonic loops is transformed to an increasing or decreasing nature when the baryonic loop contribution is added. Moreover, the divergence problem of $\lambda_{\pi(NB)}(\mu_N)$ at low μ_N is also cured in the total mean free path for pionic component $\lambda_{\pi}(\mu_N)$. A mild μ_N dependence of the nucleonic component is observed.

At fixed values of T and μ_N , the momentum distribution of thermal widths (upper panel) and mean free paths (lower panel) for all of the components have been displayed in Fig. (6). Being equivalent to the momentum distribution for the imaginary part of optical potential (see e.g. [60,62]), thermal width of pion for any mesonic or baryonic loop exhibits a non-monotonic distribution with a peak structure along the \mathbf{k} axis. The mathematical reason can roughly be understood from the relevant Eqs. (20) and (12) as described in Ref. [60]. After adding the different NB loop contributions, each of which has similar kind of momentum distribution with different numerical strength, we get a multi-peak complex structure of $\Gamma_{\pi(NB)}(\mathbf{k})$. When we add it with the $\Gamma_{\pi(\pi M)}(\mathbf{k})$, which contains a dominating profile with one peak (due to $\pi\rho$ loop mainly), then a well behaving momentum distribution with less complex structures (solid line) is obtained. The $\Gamma_N(\mathbf{k})$ (dash-dotted line) approximately appears constant with a mild reduction with \mathbf{k} . Though we notice a divergent nature of $\lambda_{\pi(NB)}(\mathbf{k})$ outside the range of $\mathbf{k} = 0.1 - 1$ GeV but the total λ_{π} in the entire momentum range remains non-divergent or finite with an well-behaved distribution.

Using the total thermal width for pionic component, $\Gamma_{\pi}(\mathbf{k}, T, \mu_N)$ in Eq. (2) and for nucleonic component, $\Gamma_N(\mathbf{k}, T, \mu_N)$ in Eq. (3), we have obtained shear viscosities $\eta_{\pi}(T, \mu_N)$ and $\eta_N(T, \mu_N)$. They are plotted by dotted and dashed lines respectively as functions of T and μ_N in the upper panels of Fig. (7) and (8). After exhibiting a soft peak structure in the low $T (< 0.1$ GeV), $\eta_{\pi}(T)$ monotonically

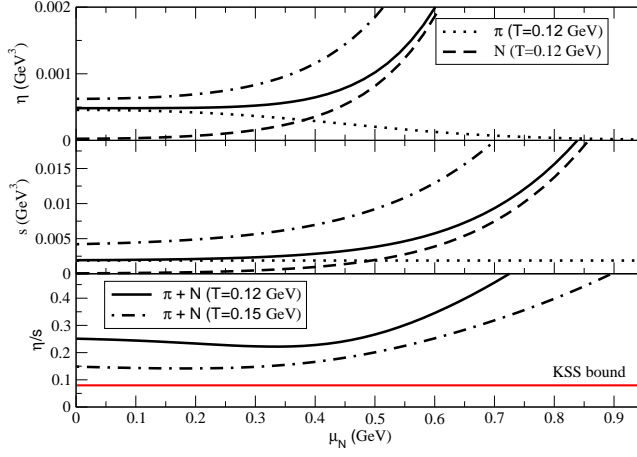


Fig. 8 The μ_N dependence of same quantities as Fig. (7) at two different temperatures: $T = 0.12$ GeV (solid line) and $T = 0.15$ GeV (dash-dotted).

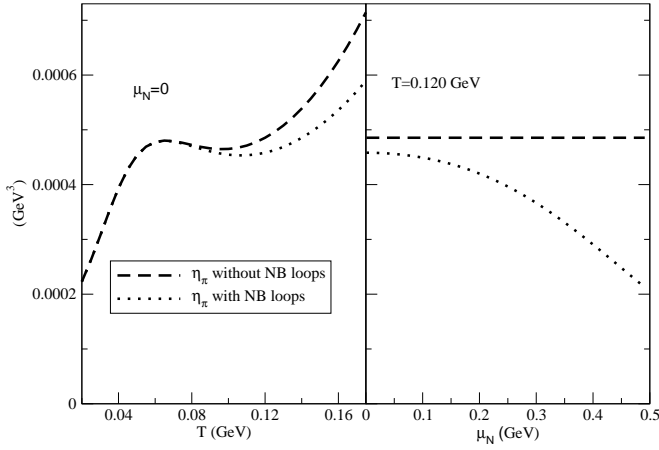


Fig. 9 Dashed and dotted lines show η_π without and with baryonic fluctuations in pion propagation respectively.

increases with a very mild rate in the high $T (> 0.1$ GeV) domain. When a monotonically increasing function $\eta_N(T)$ is added with this pionic component, the total shear viscosity η_T in high T domain enhances with slightly larger rate of increment, which can be noticed by solid line in the upper panel of Fig. (7). Another curve of $\eta_T(T)$ at $\mu_N = 0.5$ GeV is shown by dash-dotted line, which faces a rapid increment after $T = 0.06$ GeV. The reason of this drastic enhancement can be well understood from the μ_N dependence of the two components $\eta_\pi(\mu_N)$ and $\eta_N(\mu_N)$. The upper panel of Fig. (8) exposes a rapidly increasing function $\eta_N(\mu_N)$ and a soft decreasing function $\eta_\pi(\mu_N)$. Remembering the Fig. (5), we can understand that the origin of soft decreasing nature of $\eta_\pi(\mu_N)$ is coming from the baryonic loop contribution of pion as its mesonic loop contribution is independent of μ_N .

Right panel of Fig. (9) is zooming this fact more distinctly, where we see how inclusion of NB loops in pion self-energy makes η_π deviate from its independent (dashed line) to dependent (dotted line) nature with μ_N . This is the main and dramatically important contributions of the present article as an extension of earlier works [53, 54]. After including it, providing a complete picture of shear viscosity calculation for pion-nucleon system is the main aim of this present investigation.

The dotted lines in the left and right panel of Fig. (9) are exactly same as dotted lines in the upper panels of Fig. (7) and (8) respectively. Still those curves are repeated for elaborating the effect of baryonic fluctuations in pion self-energy. As the phase space factor of Eq. (2) does not depend on the μ_N , so only thermal width $\Gamma_\pi(\mu_N)$ controls on the μ_N dependence of η_π . Now between two components $\Gamma_{\pi(\pi M)}$ and $\Gamma_{\pi(NB)}$ of Γ_π , the latter one has only the dependency of μ_N as exposed in Fig. (5). The decreasing nature of $\eta_\pi(\mu_N)$ is solely governed by the increasing (decreasing) nature of function $\Gamma_\pi(\mu_N)$ ($\lambda_\pi(\mu_N)$). Whereas, in case of Eq. (3), nucleonic phase space factor depend on μ_N so strongly that it makes $\eta_N(\mu_N)$ be an increasing function after dominating over the opposite action of $\Gamma_N(\mu_N)$ or $\lambda_N(\mu_N)$ on the $\eta_N(\mu_N)$.

Middle panels of Fig. (7) and (8) represent the T and μ_N dependence of entropy densities for pionic and nucleonic components by following their ideal expressions:

$$s_\pi = 3\beta \int \frac{d^3\mathbf{k}}{(2\pi)^3} \left(\omega_k^\pi + \frac{\mathbf{k}^2}{3\omega_k^\pi} \right) n_k(\omega_k^\pi) \quad (33)$$

and

$$s_N = 4\beta \int \frac{d^3\mathbf{k}}{(2\pi)^3} \left(\omega_k^N + \frac{\mathbf{k}^2}{3\omega_k^N} - \mu_N \right) n_k^+(\omega_k^N) . \quad (34)$$

Using these numerical results of entropy densities (middle panel) as well as for shear viscosities (upper panel) for pionic, nucleonic components and their total, we have presented their corresponding ratios in the lower panels of the graphs, where straight horizontal (red) lines stand for KSS bound of the ratio. The decreasing nature of ratio is sustained for both $\mu_N = 0$ (solid line) and $\mu_N = 0.5$ GeV (dash-dotted line) in the entire T axis. The former is dominating over the later in magnitude for $T \leq 0.12$ GeV and then an opposite trend is followed beyond $T = 0.12$ GeV. Therefore, the ratio in the μ_N axis at $T = 0.15$ GeV (dash-dotted line) and $T = 0.12$ GeV (solid line) are exhibiting a nature opposite to each other (up to $\mu_N \approx 0.4$ GeV), which can be observed in the lower panel of Fig. (8). Nevertheless, both of them increase in high μ_N domain ($\mu_N > 0.4$ GeV). Most of the earlier work [33, 44, 45] showed a reducing nature of ratio along the μ_N axis, which is also found in the present work up to $T \approx 0.12$ GeV but beyond $T = 0.120$ it is not found. It indicates that our approach has some deficiency with respect to the earlier work [33, 44, 45]. This deficiency may be the mixing effect of two component system [33], which have been taken care in our further investigations and discussed in next paragraph.

We have adopted a rough mixing effect [54], which can generally be expected between two components of a mixed gas [33, 63]. From the Eqs. (2) and (3), one can clearly notice that the phase space factors of η_π and η_N do not face any mixing effect of pion density, $\rho_\pi = 3 \int \frac{d^3k}{(2\pi)^3} n_k(\omega_k^\pi)$ and nucleon density, $\rho_N = 4 \int \frac{d^3k}{(2\pi)^3} n_k^+(\omega_k^N)$. Although their thermal widths Γ_π and Γ_N contain this mixing

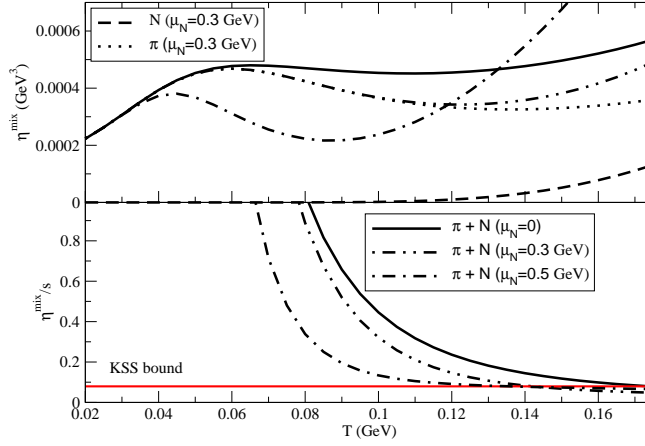


Fig. 10 Upper panel: Temperature dependence of shear viscosities of pionic (dotted line), nucleonic (dashed line) components and their total (at three different values of μ_N) in presence of mixing effect. Lower panel: The ratios of total viscosity to entropy density vs T at $\mu_N = 0$ (solid line), 0.3 GeV (dash-double-dotted line) and 0.5 GeV (dash-dotted line).

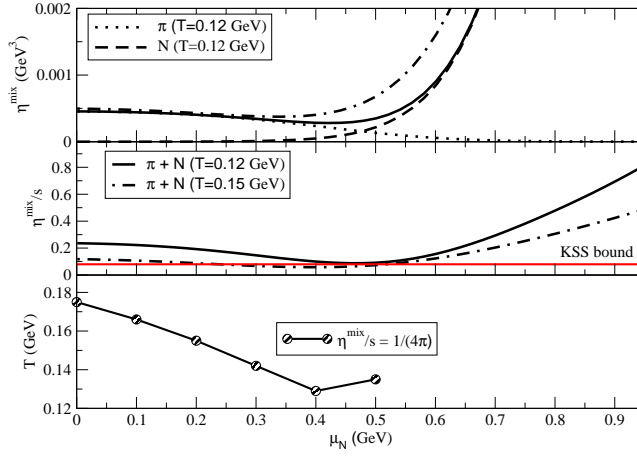


Fig. 11 upper and middle panels show the μ_N dependence of same quantities as in Fig. (10) at two different temperatures: $T = 0.12$ GeV (solid line) and $T = 0.15$ GeV (dash-dotted). Lower panel: The different points of (T, μ_N) , where η^{mix}/s is approximately equal to the KSS bound.

effect as they depend on thermal distribution functions of both, pion and nucleon. Following the approximated relation [33, 54, 63]

$$\eta_{\text{tot}}^{\text{mix}} = \eta_{\pi}^{\text{mix}} + \eta_N^{\text{mix}}, \quad (35)$$

with

$$\eta_{\pi}^{\text{mix}} = \frac{\eta_{\pi}}{1 + \left(\frac{\rho_N}{\rho_{\pi}}\right) \left(\frac{\sigma_{\pi N}}{\sigma_{\pi\pi}}\right) \sqrt{\frac{1+m_{\pi}/m_N}{2}}} \quad (36)$$

and

$$\eta_N^{\text{mix}} = \frac{\eta_N}{1 + \left(\frac{\rho_\pi}{\rho_N}\right) \left(\frac{\sigma_{\pi N}}{\sigma_{NN}}\right) \sqrt{\frac{1+m_N/m_\pi}{2}}}, \quad (37)$$

where the cross sections of all kind of scattering are simply taken as constant with same order of magnitude (*i.e.* $\sigma_{\pi\pi} \approx \sigma_{\pi N} \approx \sigma_{NN}$). In presence of this mixing scenario, the T dependence of η_π^{mix} (dotted line), η_N^{mix} (dashed line) and their total $\eta_{\text{tot}}^{\text{mix}}$ at $\mu_N = 0$ (solid line), $\mu_N = 0.3$ GeV (dash-dotted line) and $\mu_N = 0.5$ GeV are shown in the upper panel of Fig. (10). The corresponding results along the μ_N axis for two different temperatures are presented in the upper panel of Fig. (11). Lower panels of Fig. (10) and middle panel of Fig. (11) are displaying the viscosity to entropy density ratios as a function of T (at three different values of μ_N) and μ_N (at two different values of T). One should comparatively notice the dash-dotted line in the lower panel of Fig. (8) and the middle panel of Fig. (11), which are exhibiting an opposite nature in the low μ_N region. Hence the approximated T - μ_N range, where viscosity to entropy density ratio reduces, is transformed from ($T = 0 - 0.12$ GeV, $\mu_N = 0 - 0.5$ GeV) to ($T = 0 - 0.15$ GeV, $\mu_N = 0 - 0.5$ GeV) due to the mixing effect. Being closer to the earlier results [33,44,45], specially the result of Itakura et al. [33], the mixing effect appears to be very important. Though the ratios in both cases, without and with mixing effect increase beyond the $\mu_N \approx 0.5$ GeV but the conclusion of our results, based on the effective hadronic Lagrangian, should be concentrated within regions of 0.100 GeV $< T < 0.160$ GeV and $0 < \mu_N < 0.500$ GeV. The lower panel of Fig. (11) shows the T - μ_N points where the ratios are approximately equal to its KSS bound. From this plot we can get a rough idea of T - μ_N region, where our shear viscosity calculations for the pion-nucleon system may be considered as a reliable estimation by using the effective hadronic model.

4 Summary and Conclusion

The present work is an extension of our previous studies [53,54] of the shear viscosity calculations for pionic [53] and nucleonic [54] components, where pion thermal width due to different mesonic fluctuations and the nucleon thermal width due to different pion-baryon fluctuations are respectively considered. However, in the two component pion-nucleon system, pion thermal width may also be originated from different baryonic loops, which is not taken in our previous investigations [53,54]. Considering this baryonic loop contribution, we have addressed a complete picture of pion and nucleon propagation via all possible meson and baryon quantum fluctuations at finite temperature and density, from where their corresponding contributions to the shear viscosities have been found.

Following the traditional technique of Kubo relation [32,40,58,57], the shear viscosities of pion and nucleon components can be deduced from their corresponding correlators of viscous stress tensor in the static limit, which will be non-divergent when a finite thermal width will be introduced in their free propagators. These finite values of pion and nucleon thermal widths have been estimated from the RTF calculations of the pion self-energy for different mesonic and baryonic loops and the nucleon self-energy for different pion-baryon loops. Thermal width and its inverse quantity, mean free path for each component is numerically

generated as a function of the momentum \mathbf{k} of the constituent and the medium parameters, T and μ_N . They show very non-trivial momentum distributions, which have been integrated out by the Bose-enhanced and Pauli-blocked phase space factors of pion and nucleon, respectively, to calculate their corresponding shear viscosities. We have plotted the shear viscosity of each component and their total as a function of T and μ_N , where one can observe a distinct and important effect of pion thermal width for baryonic loops, which is the main finding of the present investigation to demonstrate a complete picture of shear viscosity calculation for pion-nucleon system. Actually the μ_N dependence is entering in the shear viscosity of pionic component via this baryon loop contribution of pion thermal width. This additional contribution makes the shear viscosity of pionic component reduce with μ_N and increase with T . By adopting a rough mixing effect of pion and nucleon densities between two components, we have tried to present a numerical estimation of total shear viscosity for a mixed gas of pion-nucleon constituents. Normalizing by the ideal expressions of entropy densities for pion and nucleon gas, we have obtained the viscosity to entropy density ratios for each component and their total. In the relevant T - μ_N region of hadronic domain, this ratio for the pion-nucleon gas mixture reduces and approaches toward its KSS bound as T or μ_N increases.

Acknowledgment : This work is financed by Fundação de Amparo à Pesquisa do Estado de São Paulo - FAPESP, Grant Nos. 2012/16766-0. I am very grateful to Prof. Gastao Krein for his academic and non-academic support during my postdoctoral period in Brazil.

References

1. P. Romatschke and U. Romatschke, Phys. Rev. Lett. **99**, 172301 (2007).
2. H. Song and U. W. Heinz, Phys. Lett. B **658**, 279 (2008).
3. V. Roy, A. K. Chaudhuri and B. Mohanty, Phys. Rev. C **86**, 014902 (2012)
4. H. Niemi, G.S. Denicol, P. Huovinen, E. Molnár, D.H. Rischke, Phys. Rev. Lett. **106**, 212302 (2011); Phys. Rev. C **86**, 014909 (2012).
5. B. Schenke, S. Jeon and C. Gale, Phys. Lett. B **702**, 59 (2011).
6. V. Roy, B. Mohanty, A.K. Chaudhuri, J. Phys. G **40**, 065103 (2013)
7. Z. Xu, C. Greiner, and H. Stoecker, Phys. Rev. Lett. **101**, 082302 (2008).
8. G. Ferini, M. Colonna, M. Di Toro, and V. Greco, Phys. Lett. B **670**, 325 (2009).
9. V. Greco, M. Colonna, M. Di Toro, and G. Ferini, Prog. Part. Nucl. Phys. **65**, 562 (2009).
10. J. Xu and C. M. Ko, Phys. Rev. C **84**, 014903 (2011).
11. P. Zhuang, J. Hufner, S. P. Klevansky, L. Neise Phys. Rev. D **51**, 3728 (1995); P. Rehberg, S.P. Klevansky, J. Hufner, Nucl. Phys. A **608**, 356 (1996).
12. L. P. Csernai, J. I. Kapusta, and L. D. McLerran, Phys. Rev. Lett. **97**, 152303 (2006);
13. T. Hirano and M. Gyulassy Nucl. Phys. A **769**, 71 (2006).
14. J. I. Kapusta, "Relativistic Nuclear Collisions", Landolt-Bornstein New Series, Vol. I/23, ed. R. Stock (Springer-Verlag, Berlin Heidelberg 2010).
15. J. W. Chen, M. Huang, Y. H. Li, E. Nakano, D. L. Yang, Phys. Lett. B **670**, 18 (2008);
16. P. Chakraborty and J. I. Kapusta, Phys. Rev. C **83**, 014906 (2011).
17. J.W. Chen, C.T. Hsieh, and H. H. Lin, Phys. Lett. B **701**, 327 (2011).
18. F. Karsch, E. Laermann, A. Peikert, Phys. Lett. B **478** (2000) 447.
19. A. Nakamura, S. Sakai, Phys. Rev. Lett. **94** (2005) 072305; Nucl. Phys. A **774** (2006) 775; S. Sakai, A. Nakamura, PoS LAT 2007 (2007) 221.
20. H.B. Meyer, Phys. Rev. D **76** (2007) 101701.
21. P. Kovtun, D.T. Son, and O.A. Starinets, Phys. Rev. Lett. **94**, 111601 (2005).
22. P. Arnold, G.D. Moore, L.G. Yaffe, JHEP 0011 (2000) 001; JHEP 0305 (2003) 05.
23. G. Policastro, D.T. Son, A.O. Starinets, Phys. Rev. Lett. **87** (2001) 081601.
24. G.D. Moore, JHEP 0105 (2001) 039.
25. M.A. Valle Basagoiti, Phys. Rev. D **66** (2002) 045005.

26. G. Aarts, J.M. Martinez Resco, JHEP 0211 (2002) 022.
27. S. Ghosh, A. Lahiri, S. Majumder, R. Ray, S. K. Ghosh, Phys. Rev. C **88**, 068201 (2013).
28. A. Dobado and S.N. Santalla, Phys. Rev. D **65**, 096011 (2002).
29. A. Dobado and F. J. Llanes-Estrada, Phys. Rev. D **69**, 116004 (2004).
30. A. Murgola, Phys. Rev. C **69**, 044901 (2004).
31. E. Nakano, arXiv:hep-ph/0612255; J.W. Chen, Y.H. Li, Y.F. Liu, and E. Nakano, Phys. Rev. D **76**, 114011 (2007);
32. D. Fernandez-Fraile and A. Gomez Nicola, Eur. Phys. J. C **62**, 37 (2009); Int. J. Mod. Phys. E **16**, 3010 (2007); Eur. Phys. J. A **31**, 848 (2007).
33. K. Itakura, O. Morimatsu, and H. Otomo, Phys. Rev. D **77**, 014014 (2008).
34. M.I. Gorenstein, M. Hauer, and O.N. Moroz, Phys. Rev. C **77**, 024911 (2008).
35. J.N. Hostler, J. Noronha, and C. Greiner, Phys. Rev. Lett. **103**, 172302 (2009); Phys. Rev. C **86**, 024913 (2012).
36. S. Pal, Phys. Lett. B **684**, 211 (2010).
37. A.S. Khvorostukhin, V.D. Toneev, and D.N. Voskresensky, Nucl. Phys. A **845**, 106 (2010); Phys. Atom. Nucl. **74**, 650 (2011);
38. A. Wiranata and M. Prakash, Phys. Rev. C **85**, 054908 (2012).
39. M. Buballa, K. Heckmann, J. Wambach, Prog. Part. Nucl. Phys. **67**, 348 (2012).
40. R. Lang, N. Kaiser, and W. Weise Eur. Phys. J. A **48**, 109 (2012).
41. S. Mitra, S. Ghosh, and S. Sarkar Phys. Rev. C **85**, 064917 (2012); S. Mitra, U. Gangopadhyaya, S. Sarkar, arXiv:1504.00184 [hep-ph].
42. J. Peralta-Ramos and G. Krein, Int. J. Mod. Phys. Conf. Ser. **18**, 204 (2012); Phys. Rev. C **84**, 044904 (2011).
43. A. Wiranata, V. Koch, M. Prakash, and X.N. Wang, arXiv:1307.4681 [hep-ph].
44. G.S. Denicol, C. Gale, S. Jeon, J. Noronha, Phys. Rev. C **88** (2013) 064901.
45. N. Demir and S. A. Bass, Phys. Rev. Lett. **102**, 172302 (2009).
46. G. P. Kadam, H. Mishra, Nucl. Phys. A **934** (2014) 133.
47. S. Gavin, Nucl. Phys. A **435**, 826 (1985).
48. M. Prakash, M. Prakash, R. Venugopalan, and G. Welke, Phys. Rep. **227**, 321 (1993).
49. J.L. Anderson, H.R. Witting, Physica **74** (1973) 466; Physica **74** (1973) 489.
50. V.M. Galitsky, Yu.B. Ivanov, V.A. Khangulian, Sov. J. Nucl. Phys. **30** (1979) 401.
51. P. Danielewicz, Phys. Lett. B **146** (1984) 168.
52. R. Hakim, L. Mornas, P. Peter, H.D. Sivak, Phys. Rev. D **46** (1992) 4603; R. Hakim, L. Mornas, Phys. Rev. C **47** (1993) 2846.
53. S. Ghosh, G. Krein, S. Sarkar, Phys. Rev. C **89** (2014) 045201.
54. S. Ghosh, Phys. Rev. C **90**, 025202 (2014).
55. D. N. Zubarev *Non-equilibrium statistical thermodynamics* (New York, Consultants Bureau, 1974).
56. R. Kubo, J. Phys. Soc. Jpn. **12**, 570 (1957).
57. S. Ghosh, Int. J. Mod. Phys. A **29** (2014) 1450054.
58. S. Sarkar, Advances in High Energy Physics, vol. 2013, Article ID 627137, (2013).
59. M. Post, S. Leupold, U. Mosel, Nucl. Phys. A **741**, 81 (2004).
60. S. Ghosh, J. Phy. G **41**, 095102 (2014).
61. F. Klingl, N. Kaiser, W. Weise, Z. Phys. A **356**, 193 (1996).
62. R. Rapp, J. Wambach, Nucl. Phys. A **573** (1994) 626.
63. E. H. Kennard, *Kinetic Theory of Gases, with an Introduction to Statistical Mechanics* (McGraw-Hill, New York, 1938).